Quantum dynamics with fermion coupled coherent states: Theory and application to electron dynamics in laser fields

Quantum dynamics with fermion coupled coherent states: Theory and application to electron dynamics in laser fields

Adam Kirrander[1] and Dmitrii V. Shalashilin[2]
[1]*Laboratoire Aimé Cotton du CNRS, Université de Paris-Sud, Bâtiment 505, F-91405 Orsay, France*
[2]*School of Chemistry, University of Leeds, Leeds LS2 9JT, United Kingdom*
(Received 4 June 2011; published 9 September 2011)

We present an alternate version of the coupled-coherent-state method, specifically adapted for solving the time-dependent Schrödinger equation for multielectron dynamics in atoms and molecules. This theory takes explicit account of the exchange symmetry of fermion particles, and it uses fermion molecular dynamics to propagate trajectories. As a demonstration, calculations in the He atom are performed using the full Hamiltonian and accurate experimental parameters. Single- and double-ionization yields by 160-fs and 780-nm laser pulses are calculated as a function of field intensity in the range 10^{14}–10^{16} W/cm^2, and good agreement with experiments by Walker *et al*. is obtained. Since this method is trajectory based, mechanistic analysis of the dynamics is straightforward. We also calculate semiclassical momentum distributions for double ionization following 25-fs and 795-nm pulses at 1.5×10^{15} W/cm^2, in order to compare them with the detailed experiments by Rudenko *et al*. For this more challenging task, full convergence is not achieved. However, major effects such as the fingerlike structures in the momentum distribution are reproduced.

DOI: 10.1103/PhysRevA.84.033406 PACS number(s): 32.80.Rm

I. INTRODUCTION

The method of coupled coherent states (CCS) [1–13] has been developed previously to provide a tool for fully quantum simulation of systems with a large number of degrees of freedom. The central idea of the technique is to solve the time-dependent Schrödinger equation in a basis of frozen (i.e. constant width) trajectory-guided Gaussian wave packets. This has several advantages. First, the basis can be selected randomly, which avoids the problem of exponential growth of the quantum basis with the number of degrees of freedom. Second, the trajectory-guided basis follows the evolution of the wave function, and thus it further economizes the basis set size and computational cost. The CCS method and its variations [14,15] has been applied successfully to a number of problems, which require simulation of quantum dynamics in complex multidimensional systems, such as vibrational energy transfer [4,12], nonadiabatic dynamics in molecules [14,15], dynamics and spectra of small clusters [5,13], and tunneling in systems with many degrees of freedom [8].

Originally, CCS was developed for treating the motion of distinguishable particles, but in this paper we present a version of the method particularly suited for simulating the dynamics of fermion particles, such as electrons. In Sec. II, we give a brief overview of the CCS theory and several related techniques. Then, using logic similar to that of CCS, we derive the equations of fermion coupled coherent states (FCCS). For simplicity, we only include the derivation of the equations for two electrons, such as for the He atom. Generalizations for more than two electrons are tedious but straightforward. In Sec. III, FCCS is applied to simulations of double ionization of He in intense laser fields. It is widely accepted that "recollisions," whereby ionized electrons are driven back into the parent ion, play a crucial role in this process [16]. Due to the large amplitude of the motion of electrons in the field, simulations require very large grids, which make simulations of double ionization extremely difficult and essentially insurmountable for long-wavelength and long-duration pulses. On the contrary, a trajectory-guided basis follows the electronic wave packet very efficiently.

II. THEORY

A. Coupled coherent states and related techniques

The CCS and related approaches [17–19] represent the wave function of a system with M degrees of freedom on a basis of trajectory-guided frozen Gaussian coherent states

$$|\Psi(t)\rangle = \sum_{i=1,N} a_i(t)\,|\mathbf{Z}_i(t)\rangle, \tag{1}$$

where $|\mathbf{Z}_i(t)\rangle = \prod_{k=1\ldots M} |z_i^{(k)}(t)\rangle$ is a product of M one-dimensional (1D) coherent states. Coherent states are Gaussian wave packets

$$\langle x|z\rangle = \left(\frac{\gamma}{\pi}\right)^{\frac{1}{4}} \exp\left(-\frac{\gamma}{2}(x-q)^2 + \frac{i}{\hbar}p(x-q) + \frac{ipq}{2\hbar}\right), \tag{2}$$

with a fixed width. In Klauder's notation [20] they are labeled by a single complex number

$$z = \frac{\gamma^{\frac{1}{2}}q + i\hbar^{-1}\gamma^{-\frac{1}{2}}p}{\sqrt{2}}, \tag{3}$$

which includes the coordinate q, the momentum p, and the fixed width γ. See Ref. [7] for further details about CCS notations. In this paper, the atomic units ($\hbar = 1$) are used.

The wave function in Eq. (1) contains $(N+1)\times M$ complex parameters, namely, $N \times M$ phase-space positions, $z_i^{(k)}(t)$ of N M-dimensional coherent states, and their N amplitudes $a_i(t)$. CCS assumes that the equations for the trajectories are determined by the classical-like Hamiltonian, which is simply

an average of the full quantum Hamiltonian with the coherent state $|\mathbf{Z}_i\,(t)\rangle$

$$i\,\dot{\mathbf{Z}}_i = -\frac{\partial\,\langle\mathbf{Z}_i|\,\hat{H}\,|\mathbf{Z}_i\rangle}{\partial\mathbf{Z}_i^*}. \tag{4}$$

As shown in Refs. [21] and [22], this trajectory follows from the variational principle

$$\delta\int L\,dt = 0, \tag{5}$$

written for the Lagrangian of a single coherent state,

$$L = \langle\mathbf{Z}|i\frac{\hat{\partial}}{\partial t} - \hat{H}\,|\mathbf{Z}\rangle = i\frac{\dot{\mathbf{Z}}\,\mathbf{Z}^* - \dot{\mathbf{Z}}^*\mathbf{Z}}{2} - \langle\mathbf{Z}|\hat{H}\,|\mathbf{Z}\rangle\,. \tag{6}$$

Once the assumption about the trajectories in Eq. (4) is made, then the equations for the amplitudes can be obtained simply by substituting Eq. (1) into the Schrödinger equation. It is convenient to rewrite the amplitude as a product of the oscillating exponent and the preexponential factor

$$a_j = d_j\exp(iS_j), \tag{7}$$

where S is the action $S_j = \int L_j\,dt$. The equations for d_j are then given by

$$i\sum_j\langle\mathbf{Z}_l|\mathbf{Z}_j\rangle\dot{d}_j\exp(iS_j) = \sum_j\Delta^2\mathbf{H}'_{lj}d_j\exp(iS_j) \tag{8}$$

or in matrix form

$$i\boldsymbol{\Omega}\mathbf{E}\,\dot{\mathbf{d}} = \Delta^2\mathbf{H}'\,\mathbf{E}\mathbf{d}, \tag{9}$$

where $\boldsymbol{\Omega}_{lj} = \langle\mathbf{Z}_l\,|\,\mathbf{Z}_j\rangle$ is the overlap matrix and $\mathbf{E}$ is the diagonal matrix with the elements $\mathbf{E}_{jj} = e^{iS_j}$. The elements of the $\Delta^2\mathbf{H}'$ matrix can be written as

$$\Delta^2\mathbf{H}' = (\mathbf{H} + \boldsymbol{\Omega}\boldsymbol{L} - \dot{\boldsymbol{\Omega}}), \tag{10}$$

where $\dot{\boldsymbol{\Omega}}_{lj} = \langle\mathbf{Z}_l|\dot{\mathbf{Z}}_j\rangle$ can be calculated easily. The matrix $\Delta^2\mathbf{H}'$ has been shown to be sparse, small, and with zero diagonal. Note that this follows because the coherent state trajectories (4) are driven by the diagonal of the Hamiltonian matrix. See Ref. [7] for a detailed review of CCS working equations.

Although the CCS methodology was originally developed for the dynamics of distinguishable particles, the theory has been applied to the propagation of electronic wave functions [9,11]. An important feature of the CCS method is that it uses trajectories to guide the basis. At first glance, this may not seem to be well advised for charged particles, since classical trajectories misbehave near the singularities in the Coulomb potential. For example, in the He atom, when one of the electrons falls deep into the Coulomb well near the nucleus, it immediately gives the second electron enough energy to ionize. Because of this, nearly all classical simulations use somewhat arbitrary soft-core potentials [23,24]. However, in the CCS approach, the trajectories are not driven by the classical Hamiltonian, but by the Hamiltonian *averaged* by the Gaussian coherent states. As shown in Refs. [9] and [11], this removes the Coulomb singularity. Recently, the CCS approach in its standard nonfermionic form has been used to describe electron dynamics driven by very long laser pulses [25], and it has also served as a starting point for an alternate semiclassical approach to describe angular squeezing phenomenon in intense long-wavelength laser field electron dynamics [26].

Other methods exist which explore the advantages of trajectory-guided basis sets. The variational multiconfigurational Gaussian approach (vMCG) [17,18] treats all $(N+1)\times M$ parameters of the wave function in Eq. (1) on an equal footing and derives their equations of motion from the variational principle. However, the equations of vMCG are complicated and numerically expensive. Another option proposed by the multiple spawning (MS) method is to guide the basis set by purely classical dynamics [19], which, as discussed above, would not be a good choice for charged particles. The CCS methodology is situated between vMCG and MS and is efficient and reasonably accurate. Another group of related methods are semiclassical techniques, such as Heller's frozen Gaussians (FGs) [27] and the Herman-Kluk propagator [28–31]. They also rely on the wave function in Eq. (1) but, instead of exact quantum equations for the amplitudes, they use simple semiclassical recipes. For instance, FG [27] suggests simply keeping the preexponential factor in Eq. (7) constant, which is a remarkably good approximation. A semiclassical FG approximation can be rigorously derived from the fully quantum CCS approach by assuming that the small matrix $\Delta^2\mathbf{H}'_{lj}$ on the right-hand side of Eqs. (8) and (9) is zero. In fact, FG was a starting point for the CCS technique, which can be regarded as a correction to the FG approximation. In some cases CCS is hard to converge to the exact quantum result, but in such worst-case scenarios the method works as a semiclassical technique, always providing at least qualitative, but often almost quantitative, results.

B. Fermion CCS (FCCS)

Previously, trajectory-guided methods to solve the Schrödinger equation for large systems have been used by theoretical chemists primarily to look at quantum dynamics of chemical reactions. In this paper, we develop a version of CCS particularly suited to the dynamics of electrons, which should extend the technique to many new areas of physics. We show how to use so-called fermion molecular dynamics (FMD) [32] to guide the basis. In FMD, the Pauli principle results in additional interaction between the electrons, thus incorporating quantum exchange forces in the classical dynamics. FMD can be regarded as a generalization of Heller's FGs to fermion systems. In this paper, FMD will be used as a starting point for FCCS just as FG was a starting point for the standard CCS method. By including more relevant physics into the propagation of the basis, better convergence is obtained. For simplicity, we will consider only the case of two electrons in a singlet state with $S = 0$. Other cases are more involved, but very similar.

We start by introducing a fermion coherent state as a proper Slater determinant. Then for the case of two electrons with $S = 0$, the properly symmetrized spatial part of the two-electron fermion coherent state can be written as

$$|\alpha\rangle = \frac{|\mathbf{z}_1\rangle\,|\mathbf{z}_2\rangle + |\mathbf{z}_2\rangle\,|\mathbf{z}_1\rangle}{\sqrt{2(1+|\langle\mathbf{z}_1\,|\,\mathbf{z}_2\rangle|^2)}} = \frac{|\mathbf{z}_1\rangle\,|\mathbf{z}_2\rangle + |\mathbf{z}_2\rangle\,|\mathbf{z}_1\rangle}{\sqrt{2\,(1+a)}}. \tag{11}$$

In the above equation, $|\mathbf{z}_1\rangle$ and $|\mathbf{z}_2\rangle$ are the three-dimensional (3D) Gaussians corresponding to the electrons 1 and 2. Unlike standard CCS, where a six-dimensional (6D) coherent state representing a point in the phase space of the two electrons would simply be a product $|\mathbf{Z}\rangle = |\mathbf{z}_1\rangle\,|\mathbf{z}_2\rangle$, the different fermion frozen Gaussian $|\alpha\rangle$ has the correct permutation symmetry. Then, similar to Eq. (5), a trajectory for the fermion FG can be obtained from the variational principle with the Lagrangian for the two fermions written as

$$L^F\,(\dot{\mathbf{z}}_1,\dot{\mathbf{z}}_2,\mathbf{z}_1,\mathbf{z}_2) = \langle\alpha|\,i\frac{\hat{\partial}}{\partial t} - \hat{H}\,|\alpha\rangle\,. \tag{12}$$

After that, the trajectory of the electrons is given either by the Lagrange's equations [21] or by the equivalent Hamilton's equations [22] (see below). A straightforward calculation, given in Appendix A, yields

$$L^F = \frac{i}{2(1+a)}\sum_{j=x,y,z}\{(z_{1j}^* + az_{2j}^*)\dot{z}_{1j} - (z_{1j} + az_{2j})\dot{z}_{1j}^* + (z_{2j}^* + az_{1j}^*)\dot{z}_{2j} - (z_{2j} + az_{1j}^*)\dot{z}_{2j}^*\} - \langle\alpha|\,H\,|\alpha\rangle\,, \tag{13}$$

where $a = |\langle\mathbf{z}_1|\,\mathbf{z}_2\rangle|^2$ is the overlap of the two 3D Gaussians and

$$\langle\alpha|\,\hat{H}\,|\alpha\rangle = \frac{H(\mathbf{z}_1^*,\mathbf{z}_2^*,\mathbf{z}_1,\mathbf{z}_2) + aH(\mathbf{z}_1^*,\mathbf{z}_2^*,\mathbf{z}_2,\mathbf{z}_1)}{1+a}, \tag{14}$$

where the Hamiltonian H is calculated as in Refs. [9] and [11]. It includes the integrals of Coulomb terms with Gaussians and kinetic energy terms (see Appendix B and C). Once the Lagrangian in Eqs. (11) and (12) has been written, the equations of motion can be presented as standard Lagrange's equations [21], or, more elegantly after introduction of the momenta,

$$\begin{aligned} p_{z_{1j}} &= 2\frac{\partial L}{\partial \dot{z}_{1j}} = \frac{(z_{1j}^* + az_{2J}^*)}{(1+a)},\\ p_{z_{2j}} &= 2\frac{\partial L}{\partial \dot{z}_{2j}} = \frac{(z_{2j}^* + az_{1j}^*)}{(1+a)},\\ p_{z_{1j}^*} &= 2\frac{\partial L}{\partial \dot{z}_{1j}^*} = \frac{(z_{1j} + az_{2j})}{(1+a)},\\ p_{z_{2j}^*} &= 2\frac{\partial L}{\partial \dot{z}_{2j}^*} = \frac{(z_{2j} + az_{1j})}{(1+a)}, \end{aligned} \tag{15}$$

and in the Hamiltonian form [22]

$$\begin{vmatrix} \frac{\partial \mathbf{p}_z}{\partial \mathbf{z}} & \frac{\partial \mathbf{p}_z}{\partial \mathbf{z}^*} \\ \frac{\partial \mathbf{p}_{z^*}}{\partial \mathbf{z}} & \frac{\partial \mathbf{p}_{z^*}}{\partial \mathbf{z}^*} \end{vmatrix} \begin{vmatrix} \dot{\mathbf{z}} \\ \dot{\mathbf{z}}^* \end{vmatrix} = \begin{vmatrix} \frac{\partial\,\langle\alpha|\,\hat{H}\,|\alpha\rangle}{\partial \mathbf{z}} \\ \frac{\partial\,\langle\alpha|\,\hat{H}\,|\alpha\rangle}{\partial \mathbf{z}^*} \end{vmatrix}. \tag{16}$$

In Eq. (15) $j = x,y,z$, while indices 1 and 2 correspond to the two electrons. In Eq. (16) the 3D vector $\mathbf{z}$ is either $\mathbf{z}_1$ or $\mathbf{z}_2$ and $\mathbf{p}_z$ and $\mathbf{p}_{z^*}$ are 3D vectors with components given by Eq. (15). Thus the time derivatives of the electron's phase-space position are determined from a system of six coupled linear equations (16). In Appendix A, we derive explicit expressions for the terms in Eq. (16).

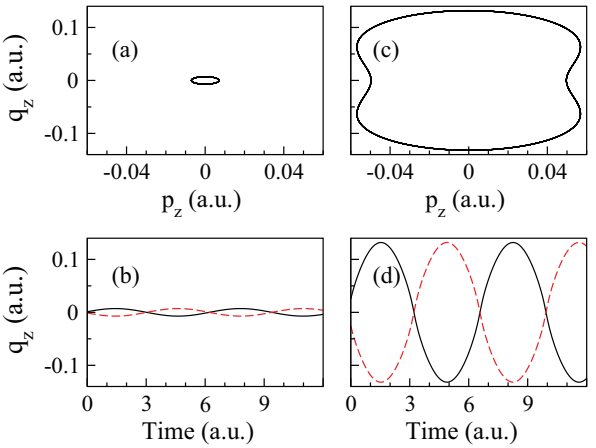

FIG. 1. (Color online) Comparison of boson trajectories [Eq. (4)] [shown in the left-hand column of (a) and (b)] with fermion trajectories [Eq. (16)] [shown in the right-hand column of (c) and (d)], at energy −2.2156 a.u., with both electrons placed symmetrically on opposite sides of the z axis, no external field, and the width of the coherent states $\gamma = 1$. The top row, (a) and (c), shows the trajectories in (p_z,q_z) space. In each case, the traces for the two electrons are identical, although traversed in the opposite sense. This can be seen in the bottom row, (b) and (d), which shows the coordinate q_z for the two electrons as functions of time (full and dashed lines). In the present low-energy example, the additional interaction due to exchange causes the fermion trajectories to occupy a larger volume in phase space [see, e.g., that the amplitude motion in (d) is larger than in (b)]. At small q_z the fermion trajectories in (c) are deformed compared to the boson trajectories in (a). In general, as the overlap a in Eq. (11) goes to zero, the difference between the boson and fermion trajectories vanishes.

Figure 1 illustrates fermion trajectories, given by Eq. (16), for the two electrons in the He atom originally positioned symmetrically on opposite sides of the nucleus, and compares them with boson trajectories, given by Eq. (4). Figure 1 clearly demonstrates the additional repulsion between fermions, which originates from the Pauli exclusion principle.

The notation aside, Eq. (16) represents well-known fermion molecular dynamics (FMD) [32]. In the remainder of this paper, this approach [32] will be referred to as fermion frozen Gaussians (FFGs) in order to distinguish it from the methodology of Ref. [33], which is known under the name fermion molecular dynamics as well. The approach [33] to fermion trajectories is based on a different mathematical framework and relies on the introduction of a physically motivated effective potential between electrons.

In FFG [32], the two fermions are dressed with frozen Gaussians, which can overlap and repel. This repulsion is derived from the variational principle. The proposal of this paper is to use FFG as a starting point for exact approaches to quantum wave function propagation, in the same way that frozen Gaussians were used as a starting point for the CCS technique. We use an ensemble of symmetrized coherent states, Eq. (11), guided by Eq. (16), as a basis. Similar to the CCS technique, we write the wave function as

$$|\Psi\rangle = \sum a_n\,|\alpha_n\rangle. \tag{17}$$

After substituting Eq. (17) into the Schrödinger equation $i\hbar\frac{d|\Psi\rangle}{dt} = \hat{H}\,|\Psi\rangle$ and closing it with $\langle\alpha_m|$, the equations for the amplitude become

$$i\hbar\sum_n \langle\alpha_m \mid \alpha_n\rangle\,\dot{a}_n = \sum_n [\langle\alpha_m|\,\hat{H}\,|\alpha_n\rangle - i\hbar\,\langle\alpha_m \mid \dot{\alpha}_n\rangle]a_n. \tag{18}$$

The equations can be rewritten in a more compact and numerically efficient form by taking the oscillating part

$$a_n = d_n \exp\left(i S_n^F\right), \tag{19}$$

where $S^F = \int L^F\,dt$ is the action with the fermion Lagrangian given by Eq. (13). After substituting Eq. (17) into Eq. (18), the latter becomes

$$i\mathbf{\Omega^F}\mathbf{E^F}\dot{\mathbf{d}} = \Delta^2\mathbf{H'^F}\mathbf{E^F}\mathbf{d}, \tag{20}$$

where, similar to the case of distinguishable (boson) particles in Eqs. (9) and (10),

$$\mathbf{\Delta^2 H'^F} = (\mathbf{H^F} + \mathbf{\Omega^F}\mathbf{L^F} - \dot{\mathbf{\Omega}}^{\mathbf{F}}), \tag{21}$$

with $\mathbf{H^F}$ and $\mathbf{\Omega^F}$ the Hamiltonian and overlap matrices, respectively,

$$\mathbf{H}^{\mathbf{F}}_{mn} = \langle\alpha_m|\,\hat{H}\,|\alpha_n\rangle\,, \quad \mathbf{\Omega}^{\mathbf{F}}_{mn} = \langle\alpha_m \mid \alpha_n\rangle\,, \tag{22}$$

and $\mathbf{E^F}$ and $\mathbf{L^F}$ are diagonal matrices of the exponentiated action and the Lagrangian according to Eq. (13), respectively,

$$\mathbf{E}^{\mathbf{F}}_{mn} = \exp\left(i S_n^F\right)\delta_{mn}, \quad \mathbf{L}^{\mathbf{F}}_{mn} = L_n\delta_{mn}. \tag{23}$$

Finally,

$$\dot{\mathbf{\Omega}}^{\mathbf{F}}_{mn} = \langle\alpha_m \mid \dot{\alpha}_n\rangle = \langle\alpha_m|\,\frac{\vec{\partial}}{\partial t}\,|\alpha_n\rangle \tag{24}$$

is calculated in Appendix B, where it is also shown that the elements of the coupling matrix $\mathbf{\Delta^2 H'^F}$ are small, the matrix is sparse, and it has zero diagonal, which provides solid ground for the fermion frozen Gaussian approximation (FFG) [32]. FFG results from FCCS if, on the right-hand side of Eq. (20), the small matrix $\mathbf{\Delta^2 H'^F}$ is assumed to be zero. If the coupling is included, Eq. (20) converts the fermion frozen Gaussians into the exact FCCS quantum technique.

Equation (20) for the coupled amplitudes of the fermion frozen Gaussians and the proof that the quantum coupling indeed represents a small correction to the FFG semiclassical approximation are the two main results of this paper. In the next section, we describe an application to the dynamics of double ionization in a strong laser field.

III. CALCULATIONS

We simulate the double ionization of the He atom using the FCCS equations presented in Sec. II. The full Hamiltonian (in atomic units) for helium, with two electrons e_1 and e_2 in 3D, is

$$\hat{H} = -\frac{\nabla^2_{e_1}}{2} - \frac{\nabla^2_{e_2}}{2} - \frac{2}{|\mathbf{r}_{e_1}|} - \frac{2}{|\mathbf{r}_{e_2}|} + \frac{1}{|\mathbf{r}_{e_1} - \mathbf{r}_{e_2}|} + \mathbf{E}(t)(\mathbf{r}_{e_1} + \mathbf{r}_{e_2}), \tag{25}$$

where the linearly polarized laser field along the z axis is given by $E(t) = A_{\rm env}(t)\,E_0\sin\omega t$, where E_0 is the maximum field intensity, ω is the angular field frequency, and $A_{\rm env}(t)$ is a trapezoidal envelope function, which remains constant at $A_{\rm env} = 1$ during a time period corresponding to the full width at half maximum (FWHM) duration of the pulse. The pulse duration was set to 160 fs (FWHM), and the wavelength was set to 780 nm, with field intensities in the range 10^{14}–10^{16} W/cm^2, corresponding to the experimental parameters of Walker *et al.* [34]. The basis used is defined by Eqs. (2) and (11), with $\gamma = 1$. First, trajectories for fermion Gaussian coherent states [Eq. (11)] were calculated for 600 000 different initial conditions, with the electrons placed symmetrically on opposite sides of the nucleus. Similar to our previous work [11], where standard (nonfermionic) CCS was used to simulate double ionization, we did not employ the entire basis of 600 000 fermion coherent states for the quantum calculation. Instead, FFG trajectories were first run in bundles of 50–200, without solving the expensive quantum coupled equations (20). Quantum probabilities for ionization were obtained by propagating the fully coupled FCCS equations [see Eq. (20)] only for bundles containing single- and double-ionization events, which were then averaged statistically assuming zero contribution from the other bundles. Calculated single- and double-ionization yields as a function of laser intensity are presented in Fig. 2. The calculations agree well with the experimental results [34], including the "knee" structure in the double-ionization yield, due to the recollision process [16]. At low intensities the agreement with experiment deteriorates, presumably due to insufficient statistics. At high intensities, the competition between single and double ionization is not fully accounted for due to the relatively small size of the bundles used in the simulations. Overall, we found that using fermion frozen Gaussian trajectories instead of those of distinguishable particles led to faster convergence and overall more accurate results than in Ref. [11]. Obtaining the double-ionization yield for such long pulses as the one used in this paper would be impossible for standard quantum-dynamics methods based on grids or static basis functions, because during the recollisions which lead to double ionization, the electrons reach distances of hundreds of atomic units from the core. Covering such a huge space would require prohibitively large grids [35]. As in our previous work using standard CCS [11], we were able to observe various mechanisms of double ionization by inspecting the trajectories. In general, these are similar to those discussed much earlier by LaGattuta and Cohen, although the fermion interaction is treated differently [36]. A selection of trajectories is shown in Fig. 3. Thus, the mechanisms originally observed in classical simulations survive in quantum dynamics as well. Note, however, that our trajectories are not simply those of classical particles, but rather they represent graphically the motion of quantum wave packets associated with the part of the wave function, which yields double ionization (and, in one example, single ionization). Figure 3(a) shows a straightforward example of sequential double ionization, and in Fig. 3(b) we see a typical recollision double ionization, where the external field drives the ionized electron back into the nucleus, leading to a simultaneous correlated escape of the two electrons at time 4100 a.u. The actual recollision occurs only after several field cycles, because of a slow breathing

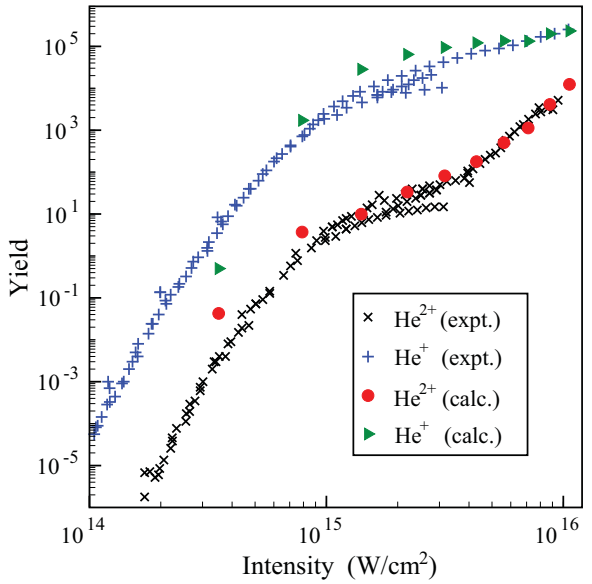

FIG. 2. (Color online) Calculated single- and double-ionization yields in He as a function of laser intensity in W/cm^2, with corresponding experimental data from Walker *et al.* [34]. The calculations use fermion dynamics (see text for details). In the calculations, the statistical error in the yield is significantly greater at low intensities.

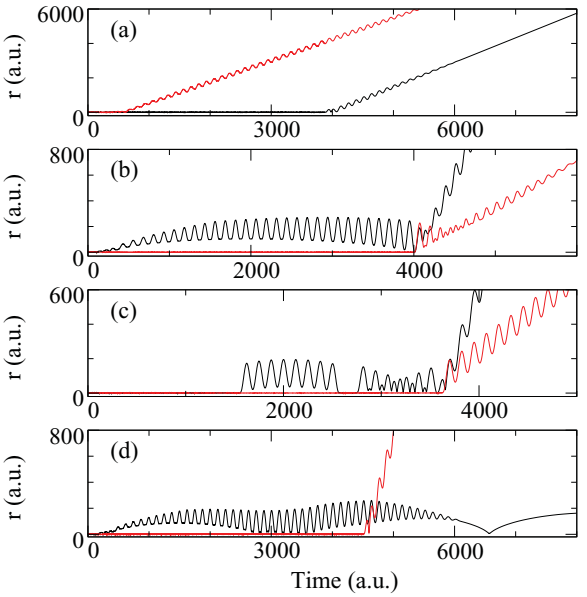

FIG. 3. (Color online) Selection of trajectories from the calculations of double ionization presented in Fig. 2. The radial distance r from the nucleus for each (indistinguishable) electron is given as a function of time. (a) Sequential double ionization for field amplitude $E = 0.30$ a.u. (b) Nonsequential double ionization due to recollision for field $E = 0.30$ a.u. The actual recollision only occurs after several field cycles, because of a slow motion of the bound electron orthogonally to the field axis. (c) An example of complicated multiple interactions between the two electrons leading to double ionization at field $E = 0.20$ a.u., including a temporary recapture of the ionized electron into an excited state at time 2560 a.u. (d) Example of interesting dynamics leading to single ionization for field $E = 0.25$ a.u., where the atom is excited into a Rydberg state at an early time. Significantly later, the second electron is ionized with the Rydberg electron acting as a spectator. The process leaves the He^+ ion in an excited Rydberg state.

motion of the bound electron orthogonally to the field axis. These kinds of "near returns" have been observed previously in trajectories calculated by LaGattuta and Cohen [36]. A minor double-ionization mechanism discussed in Ref. [11], which is also observed in the present FFG trajectories but not shown, corresponds to the case when the recollision does not immediately ionize the helium ion, but leaves it in an excited state, which is later ionized by the field. Next, in Fig. 3(c), we show an example of complicated multiple interactions between the two electrons, including a temporary recapture of the ionized electron into an excited state at time 2560 a.u., which finally leads to double ionization at time 3800 a.u. Finally, in Fig. 3(d), we show interesting single-ionization dynamics. The atom is excited into a Rydberg state early on. At a later time, the more tightly bound electron is ionized with the Rydberg electron acting as a spectator, leaving the helium ion in an excited Rydberg state at the end of the pulse. While discussing the trajectories, it is worthwhile to reiterate that the propagation in Eq. (20) couples the amplitudes of the fermion coherent states, which then collectively represent the quantum wave function in Eq. (17). Figure 4 shows the magnitude of the amplitudes for a set of 13 coherent states as a function of time, with a slowly ramped trapezoidal pulse with peak intensity 10^{16} W/cm^2. The strong quantum coupling between the different coherent states (trajectories) is apparent in the exchange of amplitude. At time 450 a.u. two trajectories ionize, leading to a loss of coupling as the ionized electrons depart from the core of the atom (see the two red arrows in Fig. 4). Throughout the simulation, the norm of the total wave function is conserved (the dashed line in Fig. 4). One (minor) consequence of norm conservation is that the average magnitude of the coherent states begins to decrease already at time 100 a.u., as the ramped field begins to distort the atom, and the trajectories explore a larger volume of space around the atom.

In a second set of calculations, we used parameters corresponding to the experiments by Rudenko *et al.* [37]. Here, a larger set of 1.2 million initial conditions was used, and only the semiclassical equations were solved [Eq. (16)]. In Fig. 5 we present the calculation of the longitudinal (i.e., along the laser polarization axis) correlated electron momentum distributions resulting from 25-fs (FWHM), 800-nm laser pulses at 1.5×10^{15} W/cm^2. The distribution shows the distinctive two-finger shape observed in experiments [37], but the distribution is too narrow, tapering off before the kinematic limits [38]. Reproducing the momentum distribution quantitatively is a challenging task. For the parameters of the pulse used by Ref. [37], the probability of double ionization is small and good statistics are required. In the future, importance sampling could be used to improve computational results. Also tunneling plays an important role. A small trajectory-guided basis cannot describe deep tunneling with high accuracy, but the basis can be adapted to tunneling better by using a spawning procedure [22,39]. Another problem is that the dynamics of the two electrons both flying away from the core after recollision might be important for a quantitative description of the

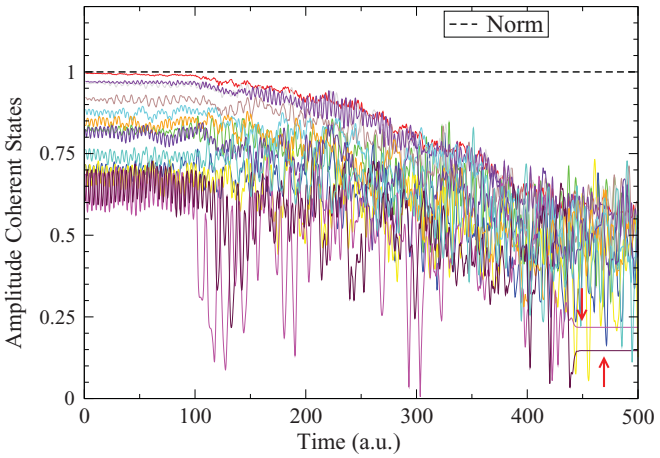

FIG. 4. (Color online) The absolute of the amplitude of the coherent states in a set of 13 coupled fermion coherent states (trajectories) during early stages of a simulation with a trapezoidal pulse with peak intensity 10^{16} W/cm^2. Note that the norm (black dashed line) of the total wave function, Eq. (17), is preserved throughout the simulation. The two red arrows indicate two trajectories which ionize at time 450 a.u. Once a coherent state is far removed from the others, the coupling becomes weak.

momentum distribution. A small bundle of trajectory-guided fermion coherent states diverge very quickly and would not be sufficient to describe fully such dynamics. To improve the quality of the dynamics, one would need to resample the basis to fill the "gaps" between diverging trajectories. From previous experience with the standard CCS method, we know that this is possible, but we have not employed these techniques yet in FCCS.

IV. DISCUSSION AND CONCLUSIONS

In Eq. (20), we show how the fermion frozen Gaussians (FFGs) [32] can be converted into a scheme for exact quantum propagation of fermion dynamics, the fermion coupled coherent states (FCCS) technique. FCCS uses a basis of properly symmetrized coherent states guided by FFG and, in addition, solves coupled equations for their amplitudes. We also show that the coupling equations are such that the coupling is always small and sparse, providing a solid base for the FFG approximation. As a practical demonstration, we calculate the strong field dynamics of helium atoms, and we compare these to experimental results for double ionization [34] and to measurements of correlated momentum distributions associated with double ionization [37]. The computational results for double-ionization yields are in good agreement with experiments. Obtaining accurate yields for such long-wavelength and long-duration pulses would be very difficult for standard quantum-dynamics methods, which use "static" grids or basis functions. The momentum distributions agree qualitatively with experiments. In this case, FCCS is used as a semiclassical technique, providing an inexpensive way to simulate complicated electron dynamics. We outline the ways to improve further the quality of FCCS simulations. Many analytical theories of strong field dynamics are based on various classical and semiclassical methods [40,41], including the quasiclassical technique of fermion molecular dynamics [33], [36] and fermion frozen Gaussians [32]. It is therefore not surprising that trajectory-based techniques can greatly help improve the efficiency of quantum simulations.

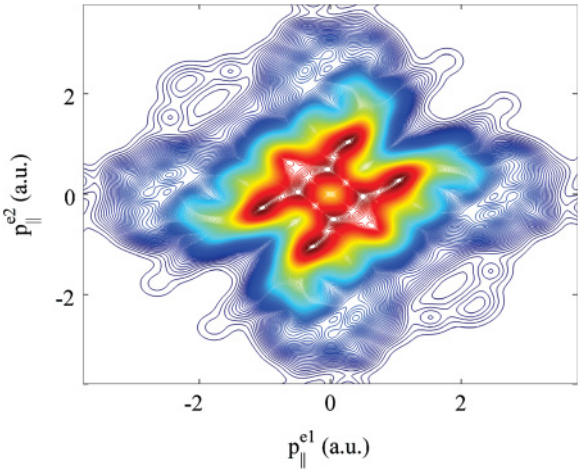

FIG. 5. (Color online) Correlated longitudinal (i.e., parallel to field axis) electron momenta corresponding to double ionization from the calculations. The distribution shows the distinctive two-finger distribution observed in experiments [37].

ACKNOWLEDGMENTS

D.S. acknowledges EPSRC Grant No. EP/I014500/1 and A.K. acknowledges support (COCOSPEC, FP7-IEF) from the European Union. We are also grateful to Jan-Michael Rost and Carla Figueira de Morisson Faria for useful discussions. Finally, we thank the referees for helpful comments.

APPENDIX A: EQUATIONS FOR FFG TRAJECTORIES

The fermion two-electron coherent state can be written as follows:

$$\begin{aligned}|\alpha\rangle &= \frac{|\mathbf{z}_1\rangle|\mathbf{z}_2\rangle + |\mathbf{z}_2\rangle|\mathbf{z}_1\rangle}{\sqrt{2(1+|\langle\mathbf{z}_1\mid\mathbf{z}_2\rangle|^2)}} \\ &= \frac{|\mathbf{z}_1\rangle|\mathbf{z}_2\rangle + |\mathbf{z}_2\rangle|\mathbf{z}_1\rangle}{\sqrt{2\left(1+\prod_{i=x,y,z} e^{z_{1i}^* z_{2i} + z_{2i}^* z_{1i} - z_{1i}^* z_{i1} - z_{2i}^* z_{2i}}\right)}} \\ &= \frac{|\mathbf{z}_1\rangle|\mathbf{z}_2\rangle + |\mathbf{z}_2\rangle|\mathbf{z}_1\rangle}{\sqrt{2\,(1+a)}}, \end{aligned} \tag{A1}$$

where $a = |\langle\mathbf{z}_1\mid\mathbf{z}_2\rangle|^2$ is the overlap of the two Gaussian coherent states dressing electrons 1 and 2. To work out the Lagrangian (13) of a single two-electron coherent state, which determines the FFG trajectories, one has to calculate $\langle\alpha|\,(i\frac{\hat{\partial}}{\partial t})\,|\alpha\rangle$, which is more conveniently done if the time derivative operator is written as the half sum $i\frac{\hat{\partial}}{\partial t} = \frac{1}{2}(i\frac{\vec{\partial}}{\partial t} - i\frac{\overleftarrow{\partial}}{\partial t})$ of two operators acting on the left-hand side and

on the right-hand side, respectively. Then

$$\langle\alpha|\left(i\frac{\vec{\partial}}{\partial t}-i\frac{\overleftarrow{\partial}}{\partial t}\right)|\alpha\rangle=\sum_{j=x,y,z}\langle\alpha|\left(i\dot{z}_{1i}\frac{\partial|\alpha\rangle}{\partial z_{1j}}+i\dot{z}_{2i}\frac{\partial|\alpha\rangle}{\partial z_{2j}}+i\dot{z}^{*}_{1j}\frac{\partial|\alpha\rangle}{\partial z*_{1j}}+i\dot{z}^{*}_{2j}\frac{\partial|\alpha\rangle}{\partial z^{*}_{2j}}\right)$$
$$-\left(i\dot{z}_{1j}\frac{\partial\langle\alpha|}{\partial z_{1j}}+i\dot{z}_{2j}\frac{\partial\langle\alpha|}{\partial z_{2j}}+i\dot{z}^{*}_{1j}\frac{\partial\langle\alpha|}{\partial z^{*}_{1j}}+i\dot{z}^{*}_{2j}\frac{\partial\langle\alpha|}{\partial z^{*}_{2j}}\right)|\alpha\rangle\,, \tag{A2}$$

where in (A2)

$$\langle\alpha|\left(i\frac{\vec{\partial}}{\partial z_{1j}}\right)|\alpha\rangle=i\frac{\langle\alpha\,(\mathbf{z}_1,\mathbf{z}_2)\,|\,\alpha(\mathbf{z}_1+\Delta z_{1j},\mathbf{z}_2)\rangle-\langle\alpha\,(\mathbf{z}_1,\mathbf{z}_2)\,|\,\alpha\,(\mathbf{z}_1,\mathbf{z}_2)\rangle}{\Delta z_{1j}}=\frac{i\,\Delta'_{1j}}{\Delta z_{1j}}. \tag{A3}$$

Now let us calculate Δ'_{1j} , where the "prime" means acting on the right-hand side, "1" means the first electron, and j means x,y,z:

$$\begin{aligned}\Delta'_{1j}&=\langle\alpha(\mathbf{z}_1,\mathbf{z}_2)\,|\,\alpha(\mathbf{z}_1+\Delta z_{1j},\mathbf{z}_2)\rangle-\langle\alpha(\mathbf{z}_1,\mathbf{z}_2)\,|\,\alpha(\mathbf{z}_1,\mathbf{z}_2)\rangle\\&=\left[\frac{\langle\mathbf{z}_1|\,\langle\mathbf{z}_2|+\langle\mathbf{z}_2|\,\langle\mathbf{z}_1|}{\sqrt{2\,(1+a)}}\frac{\left|\mathbf{z}_1+\Delta z_{1j}\right\rangle|\mathbf{z}_2\rangle+|\mathbf{z}_2\rangle\left|\mathbf{z}_1+\Delta z_{1j}\right\rangle}{\sqrt{2\,(1+a)}}+\frac{\langle\mathbf{z}_1|\,\langle\mathbf{z}_2|+\langle\mathbf{z}_2|\,\langle\mathbf{z}_1|}{\sqrt{2\,(1+a)}}\frac{|\mathbf{z}_1\rangle\,|\mathbf{z}_2\rangle+|\mathbf{z}_2\rangle\,|\mathbf{z}_1\rangle}{\sqrt{2\,(1+a+\Delta a)}}\right.\\&\quad\left.-\frac{\langle\mathbf{z}_1|\,\langle\mathbf{z}_2|+\langle\mathbf{z}_2|\,\langle\mathbf{z}_1|}{\sqrt{2\,(1+a)}}\frac{|\mathbf{z}_1\rangle\,|\mathbf{z}_2\rangle+|\mathbf{z}_2\rangle\,|\mathbf{z}_1\rangle}{\sqrt{2\,(1+a)}}\right]\\&=\left[\frac{\langle\mathbf{z}_1|\,\langle\mathbf{z}_2|+\langle\mathbf{z}_2|\,\langle\mathbf{z}_1|}{\sqrt{2\,(1+a)}}\frac{\left|\mathbf{z}_1+\Delta z_{1j}\right\rangle|\mathbf{z}_2\rangle+|\mathbf{z}_2\rangle\left|\mathbf{z}_1+\Delta z_{1j}\right\rangle}{\sqrt{2\,(1+a)}}+\frac{1+a}{2\sqrt{(1+a)\,(1+a+\Delta a)}}-1\right].\end{aligned} \tag{A4}$$

The calculation simplifies if we note that we do not need to take the term $\frac{1+a}{2\sqrt{(1+a)(1+a+\Delta a)}}$ into consideration, because the contribution from this term, from the operator $i\frac{\vec{\partial}}{\partial t}$ acting on the ket, will be canceled by a similar term with the opposite sign originating from the $-i\frac{\overleftarrow{\partial}}{\partial t}$ acting on the bra and the corresponding term

$$\langle\alpha|\left(-i\frac{\overleftarrow{\partial}}{\partial z_1}\right)|\alpha\rangle=-i\frac{\langle\alpha(\mathbf{z}_1+\Delta z_{1j},\mathbf{z}_2)\,|\,\alpha\,(\mathbf{z}_1,\mathbf{z}_2)\rangle-\langle\alpha\,(\mathbf{z}_1,\mathbf{z}_2)\,|\,\alpha\,(\mathbf{z}_1,\mathbf{z}_2)\rangle}{\Delta z_{1j}}=-\frac{i\,\Delta''_{1j}}{\Delta z_{1j}}. \tag{A5}$$

Therefore, the normalizing term a can be treated as if it were a constant. Then one only needs to calculate

$$\begin{aligned}\tilde{\Delta}'_{1j}&=\langle\alpha\,(\mathbf{z}_1,\mathbf{z}_2)\,|\,\alpha(\mathbf{z}_1+\Delta z_{1j},\mathbf{z}_2)\rangle-\langle\alpha\,(\mathbf{z}_1,\mathbf{z}_2)\,|\,\alpha\,(\mathbf{z}_1,\mathbf{z}_2)\rangle\\&=\left[\frac{\langle\mathbf{z}_1|\,\langle\mathbf{z}_2|+\langle\mathbf{z}_2|\,\langle\mathbf{z}_1|}{\sqrt{2\,(1+a)}}\frac{|\mathbf{z}_1+\Delta z_{1j}\rangle\,|\mathbf{z}_2\rangle+|\mathbf{z}_2\rangle\,|\mathbf{z}_1+\Delta z_{1j}\rangle}{\sqrt{2(1+a)}}-1\right].\end{aligned} \tag{A6}$$

Then we can get

$$\begin{aligned}\tilde{\Delta}'_{1j}&=\langle\alpha\,(\mathbf{z}_1,\mathbf{z}_2)\,|\,\alpha(\mathbf{z}_1+\Delta z_{1j},\mathbf{z}_2)\rangle-\langle\alpha\,(\mathbf{z}_1,\mathbf{z}_2)\,|\,\alpha\,(\mathbf{z}_1,\mathbf{z}_2)\rangle\\&=\frac{\langle\mathbf{z}_1|\,\langle\mathbf{z}_2|+\langle\mathbf{z}_2|\,\langle\mathbf{z}_1|}{\sqrt{2\,(1+a)}}\frac{\left|\mathbf{z}_1+\Delta z_{1j}\right\rangle|\mathbf{z}_2\rangle+|\mathbf{z}_2\rangle\left|\mathbf{z}_1+\Delta z_{1j}\right\rangle}{\sqrt{2\,(1+a)}}-1\\&=\frac{1}{2\,(1+a)}[2\langle\mathbf{z}_1\,|\,\mathbf{z}_1+\Delta z_{1j}\rangle+2\langle\mathbf{z}_2\,|\,\mathbf{z}_1+\Delta z_{1j}\rangle\,\langle\mathbf{z}_1\,|\,\mathbf{z}_2\rangle-2\,(1+\langle\mathbf{z}_2\,|\,\mathbf{z}_1\rangle\,\langle\mathbf{z}_1\,|\,\mathbf{z}_2\rangle)]\\&=\frac{1}{(1+a)}\left[\left\{1+z^{*}_{1j}\Delta z_{1j}-\frac{z^{*}_{1j}\Delta z_{1j}}{2}-\frac{z_{1j}\Delta z^{*}_{1j}}{2}\right\}+\left\{1+z^{*}_{2j}\Delta z_{1j}-\frac{z^{*}_{1j}\Delta z_{1j}}{2}-\frac{z_{1j}\Delta z^{*}_{1j}}{2}\right\}\langle\mathbf{z}_2\,|\,\mathbf{z}_1\rangle\,\langle\mathbf{z}_1\,|\,\mathbf{z}_2\rangle\right.\\&\quad\left.-\,(1+\langle\mathbf{z}_2\,|\,\mathbf{z}_1\rangle\,\langle\mathbf{z}_1\,|\,\mathbf{z}_2\rangle)\right]\\&=\frac{1}{(1+a)}\left[\left\{z^{*}_{1j}\Delta z_{1j}-\frac{z^{*}_{1j}\Delta z_{1j}}{2}-\frac{z_{1j}\Delta z^{*}_{1j}}{2}\right\}+\left\{z^{*}_{2j}\Delta z_{1j}-\frac{z^{*}_{1j}\Delta z_{1j}}{2}-\frac{z_{1j}\Delta z^{*}_{1j}}{2}\right\}\langle\mathbf{z}_2\,|\,\mathbf{z}_1\rangle\,\langle\mathbf{z}_1\,|\,\mathbf{z}_2\rangle\right],\end{aligned} \tag{A7}$$

which can be rewritten as

$$\tilde{\Delta}'_{1j}=\frac{1}{(1+a)}\left[\frac{z^{*}_{1j}\Delta z_{1j}-z_{1j}\Delta z^{*}_{1j}}{2}(1+a)+(z^{*}_{2j}-z^{*}_{1j})\Delta z_{1j}a\right]. \tag{A8}$$

Similarly,

$$\tilde{\Delta}'_{2j} = \frac{1}{(1+a)}\left[\frac{z^*_{2j}\Delta z_{2j} - z_{2j}\Delta z^*_{2j}}{2}(1+a) + (z^*_{1j} - z^*_{2j})\Delta z_{2j} a\right], \tag{A9}$$

and the terms originating from $i\frac{\overleftarrow{\partial}}{\partial t}$ are

$$\tilde{\Delta}''_{1j} = \frac{1}{(1+a)}\left[\frac{z_{1j}\Delta z^*_{1j} - z^*_{1j}\Delta z_{1j}}{2}(1+a) + (z_{2j} - z_{1j})\Delta z^*_{1j} a\right], \tag{A10}$$

$$\tilde{\Delta}''_{2j} = \frac{1}{(1+a)}\left[\frac{z_{2j}\Delta z^*_{2j} - z^*_{2j}\Delta z_{2j}}{2}(1+a) + (z_{1j} - z_{2j})\Delta z^*_{2j} a\right]. \tag{A11}$$

In total

$$\begin{aligned}
\langle\alpha|\left(i\frac{\hat{\partial}}{\partial t}\right)|\alpha\rangle &= \frac{1}{2}\langle\alpha|\left(i\frac{\vec{\partial}}{\partial t} - i\frac{\overleftarrow{\partial}}{\partial t}\right)|\alpha\rangle = \sum_{j=x,y,z}\frac{i}{2}\frac{\tilde{\Delta}'_{1j} + \tilde{\Delta}'_{2j} - \tilde{\Delta}''_{1j} - \tilde{\Delta}''_{2j}}{\Delta t} \\
&= \sum_{j=x,y,z}\frac{i}{2\Delta t}\Big\{[(z^*_{1j}\Delta z_{1j} - z_{1j}\Delta z^*_{1j}) + (z^*_{2j}\Delta z_{2j} - z_{2j}\Delta z^*_{2j})] \\
&\quad + \frac{a}{1+a}[(z_{2j} - z_{1j})(\Delta z^*_{2j} - \Delta z^*_{1j}) + (z^*_{2j} - z^*_{1j})(\Delta z_{1j} - \Delta z_{2j})]\Big\} \\
&= \sum_{j=x,y,z}\frac{i}{2}\Big\{[(z^*_{1j}\dot{z}_{1j} - z_{1j}\dot{z}^*_{1j}) + (z^*_{2j}\dot{z}_{2j} - z_{2j}\dot{z}^*_{2j})] \\
&\quad + \frac{a}{1+a}[(z_{2j} - z_{1j})(\dot{z}^*_{2j} - \dot{z}^*_{1j}) + (z^*_{2j} - z^*_{1j})(\dot{z}_{1j} - \dot{z}_{2j})]\Big\} \\
&= \frac{i}{2(1+a)}\sum_{j=x,y,z}\{(z^*_{1j} + az^*_{2j})\dot{z}_{1j} - (z_{1j} + az_{2j})\dot{z}^*_{1j} \\
&\quad + (z^*_{2j} + az^*_{1j})\dot{z}_{2j} - (z_{2j} + az^*_{1j})\dot{z}^*_{2j}\}.
\end{aligned} \tag{A12}$$

Then the Lagrangian is as follows:

$$\begin{aligned}
L = \langle\alpha|\left(i\frac{\hat{\partial}}{\partial t}\right)|\alpha\rangle - \langle\alpha|H|a\rangle &= \frac{i}{2(1+a)}\sum_{j=x,y,z}\{(z^*_{1j} + az^*_{2j})\dot{z}_{1j} - (z_{1j} + az_{2j})\dot{z}^*_{1j} \\
+ (z^*_{2j} + az^*_{1j})\dot{z}_{2j} - (z_{2j} + az^*_{1j})\dot{z}^*_{2j}\} - \langle\alpha|H|\alpha\rangle\,.
\end{aligned} \tag{A13}$$

We can now define the momenta, which are

$$p_{z_{1j}} = 2\frac{\partial L}{\partial \dot{z}_{1j}} = \frac{(z^*_{1j} + az^*_{2j})}{(1+a)}, \quad p_{z_{2j}} = 2\frac{\partial L}{\partial \dot{z}_{2j}} = \frac{(z^*_{2j} + az^*_{1j})}{(1+a)}, \tag{A14}$$

and are similar for all others:

$$p_{z^*_{1j}} = 2\frac{\partial L}{\partial \dot{z}^*_{1j}} = \frac{(z_{1j} + az_{2j})}{(1+a)}, \quad p_{z^*_{2j}} = 2\frac{\partial L}{\partial \dot{z}^*_{2j}} = \frac{(z_{2j} + az_{1j})}{(1+a)}. \tag{A15}$$

Now the elements of the matrix in Eq. (16) are

$$\begin{aligned}
\frac{\partial p_{z^*_{1j}}}{\partial z_{1j}} &= \frac{1}{1+a}\frac{\partial(z_{1j} + az_{2j})}{\partial z_{1j}} + (z_{1j} + az_{2j})\frac{\partial}{\partial z_{1j}}\left[\frac{1}{1+a}\right] \\
&= \frac{1}{1+a} + \frac{z_{2j}}{(1+a)}\frac{\partial a}{\partial z_{1j}} + \left[-\frac{(z_{1j} + az_{2j})}{(1+a)^2}\right]\frac{\partial a}{\partial z_{1j}} = \frac{1}{1+a} + \left[\frac{z_{2j} - z_{1j}}{(1+a)^2}\right]\frac{\partial a}{\partial z_{1j}} \\
&= \frac{1}{1+a} + \left[\frac{z_{2j} - z_{1j}}{(1+a)^2}\right](z^*_{2j} - z^*_{1j})a,
\end{aligned} \tag{A14a}$$

$$\frac{\partial p_{z^*_{1j}}}{\partial z^*_{1j}} = z_{2j}\frac{\partial}{\partial z^*_{1j}}\left[\frac{a}{(1+a)}\right] + z_{1j}\frac{\partial}{\partial z^*_{1j}}\left[\frac{1}{(1+a)}\right]$$

$$= z_{2j}\left[\frac{1}{(1+a)} - \frac{a}{(1+a)^2}\right]\frac{\partial a}{\partial z^*_{1j}} + z_1\left[-\frac{1}{(1+a)^2}\right]\frac{\partial a}{\partial z^*_{1j}}$$
$$= \left[\frac{1}{(1+a)^2}\right](z_{2j} - z_{1j})^2 a, \tag{A14b}$$

$$\frac{\partial p_{z^*_{1j}}}{\partial z_{2j}} = \frac{1}{1+a}\frac{\partial(z_{1j} + az_{2j})}{\partial z_{2j}} + (z_{1j} + az_{2j})\frac{\partial}{\partial z_{2j}}\left[\frac{1}{1+a}\right]$$
$$= \frac{a}{1+a} + \frac{z_{2j}}{(1+a)}\frac{\partial a}{\partial z_{2j}} + \left[-\frac{z_{1j} + az_{2j}}{(1+a)^2}\right]\frac{\partial a}{\partial z_{2j}}$$
$$= \frac{a}{1+a} + \left[\frac{z_{2j} - z_{1j}}{(1+a)^2}\right](z^*_{1j} - z^*_{2j})a, \tag{A14c}$$

$$\frac{\partial p_{z^*_{1j}}}{\partial z^*_{2j}} = \frac{1}{1+a}\frac{\partial(z_{1j} + az_{2j})}{\partial z^*_{2j}} + (z_{1j} + az_{2j})\frac{\partial}{\partial z^*_{2j}}\left[\frac{1}{1+a}\right]$$
$$\times \left[\frac{z_{2j}}{(1+a)}\right]\frac{\partial a}{\partial z^*_{2j}} + (z_{1j} + az_{2j})\left[-\frac{1}{(1+a)^2}\right]\frac{\partial a}{\partial z^*_{2j}}$$
$$= \left[\frac{1}{(1+a)^2}\right](z_{2j} - z_{1j})\frac{\partial a}{\partial z^*_{2j}}$$
$$= -\left[\frac{1}{(1+a)^2}\right](z_{2j} - z_{1j})^2 a, \tag{A14d}$$

and are similar for all others. The above equations (A14) are for z_1 and z_2, which belong to the same Cartesian degree of freedom. We also have to work out the derivative with respect to z'_1 and z'_2, where the "prime" means another Cartesian coordinate. Remember that $p_{z^*_{1j}} = 2\frac{\partial L}{\partial z^*_{1j}} = \frac{(z_{1j}+az_{2j})}{(1+a)}$, then

$$\frac{\partial p_{z^*_{1j}}}{\partial z_{1j'}} = \frac{\partial p_{z^*_{1j}}}{\partial a}\frac{\partial a}{\partial z_{1j'}}$$
$$= \left[\frac{z_{2j}}{(1+a)} - \frac{(z_{1j} + az_{2j})}{(1+a)^2}\right]\frac{\partial a}{\partial z_{1j'}} = \left[\frac{z_{2j} - z_{1j}}{(1+a)^2}\right]\frac{\partial a}{\partial z_{1j'}}$$
$$= \left[\frac{z_{2j} - z_{1j}}{(1+a)^2}\right](z^*_{2j'} - z^*_{1j'})a, \tag{A15a}$$

$$\frac{\partial p_{z^*_{1j}}}{\partial z^*_{1j'}} = \frac{\partial p_{z^*_{1j}}}{\partial a}\frac{\partial a}{\partial z^*_{1j'}}$$
$$= \left[\frac{z_{2j}}{(1+a)} - \frac{(z_{1j} + az_{2j})}{(1+a)^2}\right]\frac{\partial a}{\partial z_{1j'}} = \left[\frac{z_{2j} - z_{1j}}{(1+a)^2}\right]\frac{\partial a}{\partial z_{1j'}}$$
$$= \left[\frac{z_{2j} - z_{1j}}{(1+a)^2}\right](z_{2j'} - z_{1j'})a, \tag{A15b}$$

$$\frac{\partial p_{z^*_{1j}}}{\partial z_{2j'}} = \frac{\partial p_{z^*_{1j}}}{\partial a}\frac{\partial a}{\partial z_{2j'}}$$
$$= \left[\frac{z_{2j}}{(1+a)} - \frac{(z_{1j} + az_{2j})}{(1+a)^2}\right]\frac{\partial a}{\partial z_{1j'}} = \left[\frac{z_{2j} - z_{1j}}{(1+a)^2}\right]\frac{\partial a}{\partial z_{1j'}}$$
$$= \left[\frac{z_{2j} - z_{1j}}{(1+a)^2}\right](z^*_{1j'} - z^*_{2j'})a, \tag{A15c}$$

$$\frac{\partial p_{z^*_{1j}}}{\partial z^*_{2j'}} = \frac{\partial p_{z^*_{1j}}}{\partial a}\frac{\partial a}{\partial z^*_{2j'}}$$
$$= \left[\frac{z_{2j}}{(1+a)} - \frac{(z_{1j}+az_{2j})}{(1+a)^2}\right]\frac{\partial a}{\partial z_{1j'}} = \left[\frac{z_{2j}-z_{1j}}{(1+a)^2}\right]\frac{\partial a}{\partial z_{1j'}}$$
$$= \left[\frac{z_{2j}-z_{1j}}{(1+a)^2}\right](z_{1j'}-z_{2j'})a. \tag{A15d}$$

The Hamiltonian

$$\langle\alpha|\hat{H}|\alpha\rangle = \frac{H(\mathbf{z}^*_1,\mathbf{z}^*_2,\mathbf{z}_1,\mathbf{z}_2) + aH(\mathbf{z}^*_1,\mathbf{z}^*_2,\mathbf{z}_2,\mathbf{z}_1)}{1+a} \tag{A16}$$

because

$$\begin{aligned} H(\mathbf{z}^*_1,\mathbf{z}^*_2,\mathbf{z}_1,\mathbf{z}_2) &= H(\mathbf{z}^*_2,\mathbf{z}^*_1,\mathbf{z}_2,\mathbf{z}_1),\\ H(\mathbf{z}^*_1,\mathbf{z}^*_2,\mathbf{z}_2,\mathbf{z}_1) &= H(\mathbf{z}^*_2,\mathbf{z}^*_1,\mathbf{z}_1,\mathbf{z}_2). \end{aligned} \tag{A17}$$

For Hamilton's equations we need

$$\begin{aligned} \frac{\partial\langle\hat{H}\rangle}{\partial z^*_{1j}} &= \frac{1}{1+a}\frac{\partial H(z^*_1,z^*_2,z_1,z_2)}{\partial z^*_{1j}} + \frac{a}{1+a}\frac{\partial H(z^*_1,z^*_2,z_2,z_1)}{\partial z^*_{1j}}\\ &+ H(z^*_1,z^*_2,z_1,z_2)\frac{\partial}{\partial z^*_{1j}}\left(\frac{1}{1+a}\right)\\ &+ H(z^*_1,z^*_2,z_2,z_1)\frac{\partial}{\partial z^*_{1j}}\left(\frac{a}{1+a}\right), \end{aligned} \tag{A18}$$

where

$$\begin{aligned} \frac{\partial}{\partial z^*_{1j}}\left(\frac{1}{1+a}\right) &= -\frac{1}{(1+a)^2}(z^*_{2j}-z^*_{1j})a,\\ \frac{\partial}{\partial z^*_{1j}}\left(\frac{a}{1+a}\right) &= \left[\frac{1}{1+a} - \frac{a}{(1+a)^2}\right](z^*_{2j}-z^*_{1j})a\\ &= \frac{1}{(1+a)^2}(z^*_{2j}-z^*_{1j})a. \end{aligned} \tag{A19}$$

The above equations provide all elements for the Hamilton's equations

$$\begin{vmatrix} \frac{\partial \mathbf{p}_\mathbf{z}}{\partial \mathbf{z}} & \frac{\partial \mathbf{p}_\mathbf{z}}{\partial \mathbf{z}^*}\\ \frac{\partial \mathbf{p}_{\mathbf{z}^*}}{\partial \mathbf{z}} & \frac{\partial \mathbf{p}_{\mathbf{z}^*}}{\partial \mathbf{z}^*} \end{vmatrix} \begin{vmatrix} \dot{\mathbf{z}}\\ \dot{\mathbf{z}}^* \end{vmatrix} = \begin{vmatrix} \frac{\partial \langle H\rangle}{\partial \mathbf{z}}\\ \frac{\partial \langle H\rangle}{\partial \mathbf{z}^*} \end{vmatrix}. \tag{A20}$$

for the FFG trajectories. Each element in (A20) is either a 6D vector or a 6×6 matrix.

APPENDIX B: EQUATIONS FOR THE AMPLITUDES

Now let us work out the equations for the amplitudes by substituting the wave function (17) into the Schrödinger equation

$$i\hbar\frac{d|\Psi\rangle}{dt} = \hat{H}|\Psi\rangle, \tag{B1}$$

which yields

$$\begin{aligned} i\hbar\frac{d}{dt}\sum a_n|\alpha_n\rangle &= i\hbar\sum[\dot{a}_n|\alpha_n\rangle + a_n|\dot{\alpha}_n\rangle]\\ &= \hat{H}\sum a_n|\alpha_n\rangle. \end{aligned} \tag{B2}$$

Hence,

$$\begin{aligned} &i\hbar\sum_n\langle\alpha_m\mid\alpha_n\rangle\dot{a}_n\\ &\quad= \sum_n[\langle\alpha_m|\hat{H}|\alpha_n\rangle - i\hbar\langle\alpha_m\mid\dot{\alpha}_n\rangle]a_n. \end{aligned} \tag{B3}$$

Now we can also write the amplitude as $a_n = d_n e^{\frac{iS^F_n}{\hbar}}$ so that (B3) becomes

$$\begin{aligned} &i\hbar\sum_n\langle\alpha_m\mid\alpha_n\rangle\dot{d}_n e^{i\frac{S^F_n}{\hbar}} - \sum_n\langle\alpha_m\mid\alpha_n\rangle d_n e^{i\frac{S^F_n}{\hbar}}L^F_n\\ &\quad= \sum_n[\langle\alpha_m|\hat{H}|\alpha_n\rangle - i\hbar\langle\alpha_m\mid\dot{\alpha}_n\rangle]d_n e^{i\frac{S^F_n}{\hbar}}. \end{aligned} \tag{B4}$$

In matrix form this can be written as

$$i\boldsymbol{\Omega}^\mathbf{F}\mathbf{E}^\mathbf{F}\dot{\mathbf{d}} = (\mathbf{H}^\mathbf{F} + \boldsymbol{\Omega}^\mathbf{F}\mathbf{L}^\mathbf{F} - \dot{\boldsymbol{\Omega}}^\mathbf{F})\mathbf{E}^\mathbf{F}\mathbf{d}, \tag{B5}$$

where $\mathbf{H}^\mathbf{F}$ and $\boldsymbol{\Omega}^\mathbf{F}$ are the matrixes of the Hamiltonian and overlap, and then

$$\mathbf{H}^\mathbf{F}_{mn} = \langle\alpha_m|\hat{H}|\alpha_n\rangle, \quad \boldsymbol{\Omega}^\mathbf{F}_{mn} = \langle\alpha_m\mid\alpha_n\rangle. \tag{B6}$$

$\mathbf{E}^\mathbf{F}$ and $\mathbf{L}^\mathbf{F}$ are the diagonal matrixes

$$\begin{aligned} \mathbf{E}^\mathbf{F}_{mn} &= e^{i\frac{S_n}{\hbar}}\delta_{mn}, \quad \mathbf{L}^\mathbf{F}_{mn} = L^\mathbf{F}_n\delta_{mn},\\ \dot{\boldsymbol{\Omega}}^\mathbf{F}_{mn} &= \langle\alpha_m\mid\dot{\alpha}_n\rangle = \langle\alpha_m|\frac{\vec{\partial}}{\partial t}|\alpha_n\rangle \end{aligned} \tag{B7}$$

of action and Lagrangian and the time derivative overlap matrix.

Note that the diagonal of the matrix $(\mathbf{H}^\mathbf{F} + \boldsymbol{\Omega}^\mathbf{F}\mathbf{L}^\mathbf{F} - \dot{\boldsymbol{\Omega}}^\mathbf{F})$ is going to be equal to zero just as for the standard CCS. Indeed,

$$\langle\alpha_n|\hat{H}|\alpha_n\rangle + L_n - i\hbar\langle\alpha_m\mid\dot{\alpha}_n\rangle = 0 \tag{B8}$$

because the Lagrangian is

$$\begin{aligned} L_n &= i\hbar\langle\alpha_n\mid\dot{\alpha}_n\rangle - \langle\alpha_n|\hat{H}|\alpha_n\rangle\\ &= -i\hbar\langle\dot{\alpha}_n\mid\alpha_n\rangle - \langle\alpha_n|\hat{H}|\alpha_n\rangle\\ &= i\hbar\frac{\langle\alpha_n\mid\dot{\alpha}_n\rangle - \langle\dot{\alpha}_n\mid\alpha_n\rangle}{2} - \langle\alpha_n|\hat{H}|\alpha_n\rangle. \end{aligned} \tag{B9}$$

Equation (B9) requires proof. This is long but simple. Let us calculate

$$\langle\alpha\mid\dot{\alpha}\rangle = \langle\alpha|\frac{\vec{\partial}}{\partial t}|\alpha\rangle = \frac{\tilde{\Delta}_1}{\Delta t} + \frac{\tilde{\Delta}_2}{\Delta t} + \frac{1+a}{\sqrt{1+a}}\frac{\partial}{\partial t}\frac{1}{\sqrt{1+a}} \tag{B10}$$

and show that it is equal to $\frac{\langle\alpha_n|\dot{\alpha}_n\rangle - \langle\dot{\alpha}_n|\alpha_n\rangle}{2}$, which was used to calculate the Lagrangian (A13). We can write

$$\frac{d}{dt}\frac{1}{\sqrt{1+a}} = -\frac{1}{2(1+a)^{3/2}}\frac{da}{dt}$$
$$= -\frac{a}{2(1+a)^{3/2}}\sum_{j=x,y,z}[\dot z_{1j}(z^*_{2j}-z^*_{1j})+\dot z_{2j}(z^*_{1j}-z^*_{2j})-\dot z^*_{1j}(z_{2j}-z_{1j})-\dot z^*_{2j}(z_{1j}-z_{2j})]$$
$$= -\frac{a}{2(1+a)^{3/2}}[\dot{\mathbf{z}}_1(\mathbf{z}^*_2-\mathbf{z}^*_1)+\dot{\mathbf{z}}_2(\mathbf{z}^*_1-\mathbf{z}^*_2)-\dot{\mathbf{z}}^*_1(\mathbf{z}_2-\mathbf{z}_1)-\dot{\mathbf{z}}^*_2(\mathbf{z}_1-\mathbf{z}_2)] \tag{B11}$$

and also

$$\langle\alpha|\frac{\vec\partial}{\partial t}|\alpha\rangle = \sum_{j=x,y,z}\frac{\tilde\Delta'_{1j}}{\Delta t}+\frac{\tilde\Delta'_{2j}}{\Delta t}+\frac{1+a}{\sqrt{1+a}}\frac{\partial}{\partial t}\frac{1}{\sqrt{1+a}}$$
$$= \sum_{j=x,y,z}\frac{1}{(1+a)}\left[\frac{z^*_{1j}\dot z_{1j}-z_{1j}\dot z^*_{1j}}{2}(1+a)+(z^*_{2j}-z^*_{1j})\dot z_{1j}a\right]$$
$$+\frac{1}{(1+a)}\left[\frac{z^*_{2j}\dot z_{2j}-z_{2j}\dot z^*_{2j}}{2}(1+a)+(z^*_{1j}-z^*_{2j})\dot z_{2j}a\right]$$
$$-\frac{a}{2(1+a)}[\dot z_{1j}(z^*_{2j}-z^*_{1j})+\dot z_{2j}(z^*_{1j}-z^*_{2j})-\dot z^*_{1j}(z_{2j}-z_{1j})-\dot z^*_{2j}(z_{1j}-z_{2j})]$$
$$= \frac{i}{2(1+a)}\sum_{j=x,y,z}\{(z^*_{1j}+az^*_{2j})\dot z_{1j}-(z_{1j}+az_{2j})\dot z^*_{1j}$$
$$+(z^*_{2j}+az^*_{1j})\dot z_{2j}-(z_{2j}+az^*_{1j})\dot z^*_{2j}\}. \tag{B12}$$

As in (A12), QED. Indeed, in (B12),

$$\frac{1}{(1+a)}\left[\frac{z^*_{1j}\dot z_{1j}}{2}(1+a)+(z^*_{2j}-z^*_{1j})\dot z_{1j}a-\dot z_{1j}\frac{a}{2}(z^*_{2j}-z^*_{1j})\right]=\frac{1}{2(1+a)}\dot z_{1j}(z^*_{1j}+az^*_{2j}), \tag{B13}$$

and similarly for other terms. Therefore, Eqs. (B3)–(B5) give the fermion CCS equations for the amplitudes. They convert FFG (A20) into formally exact quantum mechanics.

To complete the formalism we also need to calculate the nondiagonal elements of the matrix $\dot{\mathbf{\Omega}}^{\mathbf{F}}_{nm} = \langle\alpha_m|\dot\alpha_n\rangle$:

$$\dot{\mathbf{\Omega}}^{\mathbf{F}}_{nm} = \langle\alpha_n\,|\,\dot\alpha_m\rangle = \langle\alpha_n|\frac{\vec\partial}{\partial t}|\alpha_m\rangle$$
$$= \left(\langle\mathbf{z}_{1n}|\langle\mathbf{z}_{2n}|\frac{\vec\partial}{\partial t}|\mathbf{z}_{1m}\rangle|\mathbf{z}_{2m}\rangle+\langle\mathbf{z}_{1n}|\langle\mathbf{z}_{2n}|\frac{\vec\partial}{\partial t}|\mathbf{z}_{2m}\rangle|\mathbf{z}_{1m}\rangle+\langle\mathbf{z}_{2n}|\langle\mathbf{z}_{1n}|\frac{\vec\partial}{\partial t}|\mathbf{z}_{1m}\rangle|\mathbf{z}_{2m}\rangle+\langle\mathbf{z}_{2n}|\langle\mathbf{z}_{1n}|\frac{\vec\partial}{\partial t}|\mathbf{z}_{2m}\rangle|\mathbf{z}_{1m}\rangle\right)$$
$$\times\frac{1}{\sqrt{1+a_n}}\frac{1}{\sqrt{1+a_m}}+(\langle\mathbf{z}_{1n}|\langle\mathbf{z}_{2n}|+\langle\mathbf{z}_{2n}|\langle\mathbf{z}_{1n}|(|\mathbf{z}_{1m}\rangle|\mathbf{z}_{2m}\rangle+|\mathbf{z}_{2m}\rangle|\mathbf{z}_{1m}\rangle))\frac{1}{\sqrt{1+a_n}}\frac{d}{dt}\left(\frac{1}{\sqrt{1+a_m}}\right)$$
$$= \left(\langle\mathbf{z}_{1n}|\langle\mathbf{z}_{2n}|\frac{\vec\partial}{\partial t}|\mathbf{z}_{1m}\rangle|\mathbf{z}_{2m}\rangle+\langle\mathbf{z}_{1n}|\langle\mathbf{z}_{2n}|\frac{\vec\partial}{\partial t}|\mathbf{z}_{2m}\rangle|\mathbf{z}_{1m}\rangle+\langle\mathbf{z}_{2n}|\langle\mathbf{z}_{1n}|\frac{\vec\partial}{\partial t}|\mathbf{z}_{1m}\rangle|\mathbf{z}_{2m}\rangle+\langle\mathbf{z}_{2n}|\langle\mathbf{z}_{1n}|\frac{\vec\partial}{\partial t}|\mathbf{z}_{2m}\rangle|\mathbf{z}_{1m}\rangle\right)$$
$$\times\frac{1}{\sqrt{1+a_n}}\frac{1}{\sqrt{1+a_m}}-\langle\alpha_n\,|\,\alpha_m\rangle\frac{\dot a_m}{2(1+a_m)}. \tag{B14}$$

Let us now find

$$\langle\mathbf{z}_{1n}|\langle\mathbf{z}_{2n}|\frac{\vec\partial}{\partial t}|\mathbf{z}_{1m}\rangle|\mathbf{z}_{2m}\rangle = \langle\mathbf{z}_{1n}|\frac{\vec\partial}{\partial t}|\mathbf{z}_{1m}\rangle\langle\mathbf{z}_{2n}\,|\,\mathbf{z}_{2m}\rangle+\langle\mathbf{z}_{1n}\,|\,\mathbf{z}_{1m}\rangle\langle\mathbf{z}_{2n}|\frac{\vec\partial}{\partial t}|\mathbf{z}_{2m}\rangle$$
$$= \frac{\langle\mathbf{z}_{2n}\,|\,\mathbf{z}_{2m}\rangle}{\Delta t}\left[e^{\mathbf{z}^*_{1n}(\mathbf{z}_{1m}+\Delta\mathbf{z}_{1m})-\frac{\mathbf{z}^*_{1n}\mathbf{z}_{1n}}{2}-\frac{(\mathbf{z}^*_{1m}+\Delta\mathbf{z}^*_{1m})(\mathbf{z}_{1m}+\Delta\mathbf{z}_{1m})}{2}}-e^{\mathbf{z}^*_{1n}\mathbf{z}_{1m}-\frac{\mathbf{z}^*_{1n}\mathbf{z}_{1n}}{2}-\frac{\mathbf{z}^*_{1m}\mathbf{z}_{1m}}{2}}\right]$$
$$+\frac{\langle\mathbf{z}_{1n}\,|\,\mathbf{z}_{1m}\rangle}{\Delta t}\left[e^{\mathbf{z}^*_{2n}(\mathbf{z}_{2m}+\Delta\mathbf{z}_{2m})-\frac{\mathbf{z}^*_{2n}\mathbf{z}_{2n}}{2}-\frac{(\mathbf{z}^*_{2m}+\Delta\mathbf{z}^*_{2m})(\mathbf{z}_{2m}+\Delta\mathbf{z}_{2m})}{2}}-e^{\mathbf{z}^*_{2n}\mathbf{z}_{2m}-\frac{\mathbf{z}^*_{2n}\mathbf{z}_{2n}}{2}-\frac{\mathbf{z}^*_{2m}\mathbf{z}_{2m}}{2}}\right]$$
$$= \frac{\langle\mathbf{z}_{1n}\,|\,\mathbf{z}_{1m}\rangle\langle\mathbf{z}_{2n}\,|\,\mathbf{z}_{2m}\rangle}{\Delta t}\left[\left(e^{\mathbf{z}^*_{1n}\Delta\mathbf{z}_{1m}-\frac{\mathbf{z}^*_{1m}\Delta\mathbf{z}_{1m}+\mathbf{z}_{1m}\Delta\mathbf{z}^*_{1m}}{2}}-1\right)+\left(e^{\mathbf{z}^*_{2n}\Delta\mathbf{z}_{2m}-\frac{\mathbf{z}^*_{2m}\Delta\mathbf{z}_{2m}+\mathbf{z}_{2m}\Delta\mathbf{z}^*_{2m}}{2}}-1\right)\right]$$
$$= \langle\mathbf{z}_{1n}\,|\,\mathbf{z}_{1m}\rangle\langle\mathbf{z}_{2n}\,|\,\mathbf{z}_{2m}\rangle\left[\left(\mathbf{z}^*_{1n}\dot{\mathbf{z}}_{1m}-\frac{\mathbf{z}^*_{1m}\dot{\mathbf{z}}_{1m}+\mathbf{z}_{1m}\dot{\mathbf{z}}^*_{1m}}{2}\right)+\left(\mathbf{z}^*_{2n}\dot{\mathbf{z}}_{2m}-\frac{\mathbf{z}^*_{2m}\dot{\mathbf{z}}_{2m}+\mathbf{z}_{2m}\dot{\mathbf{z}}^*_{2m}}{2}\right)\right]$$

$$= \langle \mathbf{z}_{1n} \mid \mathbf{z}_{1m}\rangle\langle \mathbf{z}_{2n} \mid \mathbf{z}_{2m}\rangle\left[(\mathbf{z}^*_{1n} - \mathbf{z}^*_{1m})\dot{\mathbf{z}}_{1m} + \frac{\mathbf{z}^*_{1m}\dot{\mathbf{z}}_{1m} - \mathbf{z}_{1m}\dot{\mathbf{z}}^*_{1m}}{2} + (\mathbf{z}^*_{2n} - \mathbf{z}^*_{2m})\dot{\mathbf{z}}_{2m} + \frac{\mathbf{z}^*_{2m}\dot{\mathbf{z}}_{2m} - \mathbf{z}_{2m}\dot{\mathbf{z}}^*_{2m}}{2}\right]. \tag{B15a}$$

Similarly,

$$\langle \mathbf{z}_{1n}|\langle \mathbf{z}_{2n}|\tfrac{\vec{\partial}}{\partial t}|\mathbf{z}_{2m}\rangle|\mathbf{z}_{1m}\rangle = \langle \mathbf{z}_{1n} \mid \mathbf{z}_{2m}\rangle\langle \mathbf{z}_{2n} \mid \mathbf{z}_{1m}\rangle\left[(\mathbf{z}^*_{1n} - \mathbf{z}^*_{2m})\dot{\mathbf{z}}_{2m} + \frac{\mathbf{z}^*_{2m}\dot{\mathbf{z}}_{2m} - \mathbf{z}_{2m}\dot{\mathbf{z}}^*_{2m}}{2} + (\mathbf{z}^*_{2n} - \mathbf{z}^*_{1m})\dot{\mathbf{z}}_{1m} + \frac{\mathbf{z}^*_{1m}\dot{\mathbf{z}}_{1m} - \mathbf{z}_{1m}\dot{\mathbf{z}}^*_{1m}}{2}\right], \tag{B15b}$$

$$\langle \mathbf{z}_{2n}|\langle \mathbf{z}_{1n}|\tfrac{\vec{\partial}}{\partial t}|\mathbf{z}_{2m}\rangle|\mathbf{z}_{1m}\rangle = \langle \mathbf{z}_{2n} \mid \mathbf{z}_{2m}\rangle\langle \mathbf{z}_{1n} \mid \mathbf{z}_{1m}\rangle\left[(\mathbf{z}^*_{2n} - \mathbf{z}^*_{2m})\dot{\mathbf{z}}_{2m} + \frac{\mathbf{z}^*_{2m}\dot{\mathbf{z}}_{2m} - \mathbf{z}_{2m}\dot{\mathbf{z}}^*_{2m}}{2} + (\mathbf{z}^*_{1n} - \mathbf{z}^*_{1m})\dot{\mathbf{z}}_{1m} + \frac{\mathbf{z}^*_{1m}\dot{\mathbf{z}}_{1m} - \mathbf{z}_{1m}\dot{\mathbf{z}}^*_{1m}}{2}\right], \tag{B15c}$$

$$\langle \mathbf{z}_{2n}|\langle \mathbf{z}_{1n}|\tfrac{\vec{\partial}}{\partial t}|\mathbf{z}_{1m}\rangle|\mathbf{z}_{2m}\rangle = \langle \mathbf{z}_{2n} \mid \mathbf{z}_{1m}\rangle\langle \mathbf{z}_{1n} \mid \mathbf{z}_{2m}\rangle\left[(\mathbf{z}^*_{2n} - \mathbf{z}^*_{1m})\dot{\mathbf{z}}_{1m} + \frac{\mathbf{z}^*_{1m}\dot{\mathbf{z}}_{1m} - \mathbf{z}_{1m}\dot{\mathbf{z}}^*_{1m}}{2} + (\mathbf{z}^*_{1n} - \mathbf{z}^*_{1m})\dot{\mathbf{z}}_{2m} + \frac{\mathbf{z}^*_{2m}\dot{\mathbf{z}}_{2m} - \mathbf{z}_{2m}\dot{\mathbf{z}}^*_{2m}}{2}\right]. \tag{B15d}$$

The term $\dot{a}_m$ is actually calculated above in Eq. (B11). Only the index m should be added:

$$\frac{da_m}{dt} = a\big[\dot{\mathbf{z}}_{1m}(\mathbf{z}^*_{2m} - \mathbf{z}^*_{1m}) + \dot{\mathbf{z}}_{2m}(\mathbf{z}^*_{1m} - \mathbf{z}^*_{2m}) - \dot{\mathbf{z}}^*_{1m}(\mathbf{z}_{2m} - \mathbf{z}_{1m}) - \dot{\mathbf{z}}^*_{2m}(\mathbf{z}_{1m} - \mathbf{z}_{2m})\big]. \tag{B16}$$

This completes the formalism.

APPENDIX C: THE COULOMB INTERACTION OF TWO ELECTRONS AND ITS MATRIX ELEMENTS

The coherent state matrix elements of Coulomb interactions have been found in Refs. [9] and [11]. An immediate consequence of the Gaussian averaging is to remove the Coulomb singularity at the origin $\mathbf{R_c}$, because

$$\langle \mathbf{z}|\frac{1}{|\mathbf{r} - \mathbf{R_c}|}|\mathbf{z}'\rangle = \langle \mathbf{z} \mid \mathbf{z}'\rangle\frac{1}{\rho}\mathrm{erf}(\sqrt{\gamma}\rho), \tag{C1}$$

where $\tilde{\mathbf{n}} = \frac{\mathbf{z}^* + \mathbf{z}'}{\sqrt{2\gamma}} - \mathbf{R_c}$, $\rho = \sqrt{\tilde{\mathbf{n}}\cdot\tilde{\mathbf{n}}}$, and erf is the complex error function. Similarly, the two electron integrals were evaluated as

$$\langle \mathbf{z}_1, \mathbf{z}_2|\frac{1}{|\mathbf{r}_{12}|}|\mathbf{z}'_1, \mathbf{z}'_2\rangle = \langle \mathbf{z}_1 \mid \mathbf{z}'_1\rangle\langle \mathbf{z}_2 \mid \mathbf{z}'_2\rangle\frac{1}{\rho_{12}}\mathrm{erf}(\sqrt{\frac{\gamma}{2}}\rho_{12}), \tag{C2}$$

where $\tilde{\mathbf{n}}_{12} = \frac{\mathbf{z}^*_1 + \mathbf{z}'_1}{\sqrt{2\gamma}} - \frac{\mathbf{z}^*_2 + \mathbf{z}'_2}{\sqrt{2\gamma}}$ and $\rho_{12} = \sqrt{\tilde{\mathbf{n}}_{12}\cdot\tilde{\mathbf{n}}_{12}}$. As may be verified from Eqs. (C1) and (C2), ρ and ρ_{12} are the coherent state representations of the electron-nuclear and electron-electron separations.

[1] D. V. Shalashilin and M. S. Child, J. Chem. Phys. **113**, 10028 (2000).
[2] D. V. Shalashilin and M. S. Child, J. Chem. Phys. **114**, 9296 (2001).
[3] D. V. Shalashilin and M. S. Child, J. Chem. Phys. **115**, 5367 (2001).
[4] D. V. Shalashilin and M. S. Child, J. Chem. Phys. **119**, 1961 (2003).
[5] D. V. Shalashilin, M. S. Child, and D. C. Clary, J. Chem. Phys. **120**, 5608 (2004).
[6] D. V. Shalashilin and M. S. Child, J. Chem. Phys. **121**, 3563 (2004).
[7] D. V. Shalashilin and M. S. Child, Chem. Phys. **304**, 103 (2004).
[8] P. A. J. Sherratt, D. V. Shalashilin, and M. S. Child, Chem. Phys. **322**, 127 (2006).
[9] D. V. Shalashilin and M. S. Child, J. Chem. Phys. **122**, 224108 (2005).
[10] D. V. Shalashilin and M. S. Child J. Chem. Phys. **128**, 054102 (2008).
[11] D. V. Shalashilin, M. S. Child, and A. Kirrander, Chem. Phys. **347**, 257 (2008).
[12] S. K. Reed, D. R. Glowacki, and D. V. Shalashilin, Chem. Phys. **370**, 223 (2010).
[13] S. K. Reed, M. L. González-Martínez, J. Rubayo-Soneira, and D. V. Shalashilin J. Chem. Phys. **134**, 054110 (2011).
[14] D. V. Shalashilin, J. Chem. Phys. **130**, 244101 (2009).
[15] D. V. Shalashilin, J. Chem. Phys. **132**, 244111 (2010).
[16] P. B. Corkum, Phys. Rev. Lett. **71**, 1994 (1993).
[17] I. Burghardt, H.-D. Meyer, and L. S. Cederbaum, J. Chem. Phys. **111**, 2927 (1999).
[18] G. A. Worth and I. Burghardt, Chem. Phys. Lett. **368**, 502 (2003).
[19] M. Ben-Nun and T. J. Martinez, Adv. Chem. Phys. **121**, 439 (2002).
[20] J. R. Klauder and B. S. Skagerstam, *Coherent States* (World Scientific, Singapore, 1985).

[21] D. V. Shalashilin and I. Burghardt, J. Chem. Phys. **129**, 084104 (2008).
[22] M. Ben-Nun and T. J. Martinez, Adv. Chem. Phys. **121**, 439 (2002).
[23] J. Javanainen, J. H. Eberly, and Q. Su, Phys. Rev. A **38**, 3430 (1988).
[24] Q. Su and J. H. Eberly, Phys. Rev. A **44**, 5997 (1991).
[25] J. Guo, X-S. Liu, and Shih-I Chu, Phys. Rev. A **82**, 023402 (2010).
[26] Z. Zhou and Shih-I Chu, Phys. Rev. A **83**, 033406 (2011).
[27] E. J. Heller, J. Chem. Phys. **75**, 2923 (1981).
[28] M. F. Herman and E. Kluk, Chem. Phys. **91**, 27 (1984).
[29] E. Kluk, M. F. Herman, and H. L. Davis, J. Chem. Phys. **84**, 326 (1986).
[30] F. Grossmann, Comments At. Mol. Phys. **34**, 141 (1999).
[31] M. S. Child and D. V. Shalashilin, J. Chem. Phys. **118**, 2061 (2003).
[32] H. Feldmeier and J. Schnack, Rev. Mod. Phys. **72**, 655 (2000).
[33] K. J. LaGattuta, J. Phys. A **36**, 6013 (2003).
[34] B. Walker, B. Sheehy, L. F. DiMauro, P. Agostini, K. J. Schafer, and K. C. Kulander, Phys. Rev. Lett. **73**, 1227 (1994).
[35] J. S. Parker, B. J. S. Doherty, K. J. Meharg, and K. T. Taylor, J. Phys. B **36**, L393 (2003).
[36] K. J. LaGattuta and J. S. Cohen, J. Phys. B **31**, 5281 (1998).
[37] A. Rudenko, V. L. B. de Jesus, Th. Ergler, K. Zrost, B. Feuerstein, C. D. Schröter, R. Moshammer, and J. Ullrich, Phys. Rev. Lett. **99**, 263003 (2007).
[38] B. Feuerstein, R. Moshammer, and J. Ullrich, J. Phys. B **33**, L823 (2000).
[39] M. Ben-Nun and T. J. Martinez, J. Chem. Phys. **112**, 6113 (2000).
[40] M. Yu. Ivanov, O. V. Tikhonova, and M. V. Fedorov, Phys. Rev. A **58**, R793 (1998).
[41] Z. B. Walters and O. Smirnova, J. Phys. B **43**, 161002 (2010).